ACS APPLIED MATERIALS & INTERFACES

Research Article

www.acsami.org

Optimized Anion Exchange Membranes for Vanadium Redox Flow Batteries

Dongyang Chen,[†] Michael A. Hickner,*[,†] Ertan Agar,[‡] and E. Caglan Kumbur*[,‡]

[†]Department of Materials Science and Engineering, The Pennsylvania State University, University Park, Pennsylvania 16802, United States

[‡]Electrochemical Energy Systems Laboratory, Department of Mechanical Engineering and Mechanics, Drexel University, Philadelphia, Pennsylvania 19104, United States

Supporting Information

ABSTRACT: In order to understand the properties of low vanadium permeability anion exchange membranes for vanadium redox flow batteries (VRFBs), quaternary ammonium functionalized Radel (QA-Radel) membranes with three ion exchange capacities (IECs) from 1.7 to 2.4 mequiv g^{-1} were synthesized and 55−60 μm thick membrane samples were evaluated for their transport properties and in-cell battery performance. The ionic conductivity and vanadium permeability of the membranes were investigated and correlated to the battery performance through measurements of Coulombic efficiency, voltage efficiency and energy efficiency in single cell tests, and capacity fade during cycling. Increasing the IEC of the QA-Radel membranes increased both the ionic conductivity and VO^{2+} permeability. The 1.7 mequiv g^{-1} IEC QA-Radel had the highest Coulombic efficiency and best cycling capacity maintenance in the VRFB, while the cell's voltage efficiency was limited by the membrane's low ionic conductivity. Increasing the IEC resulted in higher voltage efficiency for the 2.0 and 2.4 mequiv g^{-1} samples, but the cells with these membranes displayed reduced Coulombic efficiency and faster capacity fade. The QA-Radel with an IEC of 2.0 mequiv g^{-1} had the best balance of ionic conductivity and VO^{2+} permeability, achieving a maximum power density of 218 mW cm^{-2} which was higher than the maximum power density of a VRFB assembled with a Nafion N212 membrane in our system. While anion exchange membranes are under study for a variety of VRFB applications, this work demonstrates that the material parameters must be optimized to obtain the maximum cell performance.

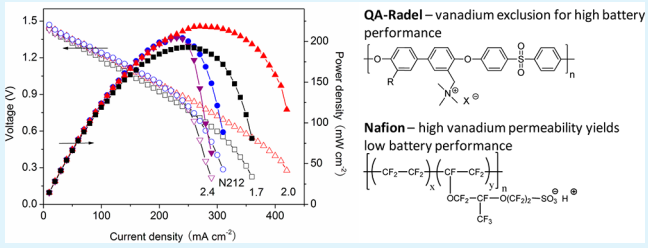

KEYWORDS: *vanadium redox flow battery, anion exchange membrane, ion exchange capacity, cycling performance, power density*

1. INTRODUCTION

Vanadium redox flow batteries (VRFBs) have attracted recent attention as a large scale energy storage system for renewable power generation because of their high energy efficiency, facile maintenance, safe operation, and low cost.[1−6] Traditional solid-state batteries such as lithium ion batteries or nickel−metal hydride batteries possess much greater specific energy density than flow batteries, but there are safety issues associated with the scaling up of these closed-system batteries for large-scale energy storage applications.[7] Flow batteries, especially all-vanadium chemistry with aqueous electrolytes that can be stored in large tanks external to the battery cell, have thus been proposed. The unique characteristic of VRFBs is that both the anolyte and catholyte employ vanadium in different valence states as the electroactive species, making the cross contamination of active species easy to correct by regeneration of the electrolyte.[8,9] To maintain high performance of the cell and promote long intervals between maintenance periods, the transport properties of the membrane should be optimized, as the crossover of vanadium ions causes capacity fade during cell operation, and the ion conductivity of the membrane influences the ohmic loss in the cell.[10−12]

Proton exchange membranes (PEMs) have been widely used in VRFBs since the vanadium-based electrolytes are generally acidic to promote vanadium species solubility.[13] Using proton conduction to balance the charge during reduction and oxidation of the vanadium redox couples can result in low ohmic losses, since aqueous electrolytes are highly proton conductive at low pH. Consequently, PEMs with moderate ion exchange capacities (IECs) usually have good ionic conductivity for VRFBs compared to other types of membrane separators.[14] The main drawback of PEMs in VRFBs is their high permeability to vanadium cations since the materials are intrinsically cation permeable.[15,16] For example, Nafion, the benchmark PEM, suffers from severe vanadium species permeation in VRFBs.[3] While the vanadium permeation can be mitigated by hybridization or blending Nafion with other components,[17−19][20] or using alternative PEMs such as randomly sulfonated poly(arylene ether)s,[21,22] the Coulombic efficiency of the VRFBs assembled with cation-conducting

Received: May 16, 2013
Accepted: June 25, 2013
Published: June 25, 2013

membranes is usually lower than the Coulombic efficiency of the VRFBs assembled with anion exchange membranes (AEMs).[23]

Anion exchange membranes contain tethered positively charged groups such as quaternary ammonium or pyridinium moieties that can repulse vanadium cations, a membrane phenomenon known as Donnan exclusion, resulting in extremely low vanadium cation permeation.[23−27] The sulfate anion (in the case of H_2SO_4-based electrolytes) or other anion in the electrolyte of the VRFB is the major charge carrier in this case, while the proton can be a minority charge carrier due to imperfect Donnan exclusion of the cations from the AEM.[28,29] The overall ionic conductivity of AEMs immersed in the vanadium electrolytes that contain a high concentration of sulfuric acid is generally much greater than the pure anion conductivity of AEM samples equilibrated in water, because of the conductivity contributions from the absorbed sulfate anions and the protons. Conversely, the overall ionic conductivity of PEMs in vanadium acidic electrolyte is lower than the pure proton conductivity of the PEMs, because some of the anionic sites in the sulfonated polymers are occupied by the low mobility vanadium cations.[23] Therefore, comparable ionic conductivity of AEMs and PEMs in VRFB electrolytes can be achieved by manipulation of their IECs and electrolyte uptake.

The species crossover through the membrane in a VRFB is important as vanadium contaminants of the wrong valence in the anolyte or catholyte will accumulate during prolonged charge−discharge cycles. Therefore, low vanadium permeability anion exchange membranes appear to be one of the most promising candidates for use as ion-exchange separators in VRFBs. While high-exclusion membranes have been demonstrated recently in VRFBs,[23] detailed information on the influence of the membrane composition and transport properties of anion exchange membranes and their relationship with the cell performance still needs to be sought to optimize these separator systems. In this work, quaternary ammonium randomly functionalized poly(arylene ether sulfone)s (Radel) with IECs from 1.7 to 2.4 mequiv g^{-1} were synthesized as the model AEMs and the membranes were systematically examined for their fundamental physicochemical properties as well as their detailed VRFB performance.

2. EXPERIMENTAL SECTION

2.1. Materials. Poly(arylene ether sulfone) resin (Radel R-5500 NT, M_w 63 kg mol^{-1}) was donated by Solvay Advanced Polymers, LLC (Alpharetta, GA). Nafion N212 was purchased from Ion Power Inc. (Bear, DE). All the other chemicals were purchased from common commercial suppliers and used as received.

2.2. Synthesis of Quaternary Ammonium Functionalized Radel (QA-Radel). As shown in Scheme 1, the synthesis of the target AEMs involved two steps, namely, chloromethylation to form the precursor benzyl halide-functionalized polymer and quaternization to yield a cationic polymer.

2.2.1. Chloromethylation of Radel. First, 4.0 g of Radel was dissolved in 100 mL of 1,1,2,2-tetrachloroethane at 60 °C in a three-neck, round-bottom flask. The solution was cooled to room temperature, and 25 mL of dimethoxylmethane (0.28 mol) was added dropwise under vigorous magnetic stirring. Then, 9.2 mL of thionyl chloride (0.13 mol) was added dropwise to the mixture, followed by the addition of 13 mL of 1 M tin(IV) chloride solution in methylene chloride. The reaction was maintained at 60 °C for varying times to control the degree of chloromethyl functionalization. The reaction mixture was poured into 1 L of methanol to precipitate a fibrous product. Materials with degrees of functionalization (DF, chloromethyl moieties per polymer repeat unit) of 0.84, 1.01, and 1.33 corresponding to final IECs of 1.7, 2.0, and 2.4 mequiv g^{-1} were obtained with reaction times of 4, 6, and 10 h, respectively.

Scheme 1. Synthesis of Quaternary Ammonium Functionalized Radel (QA-Radel) with ^{1}H Assignments

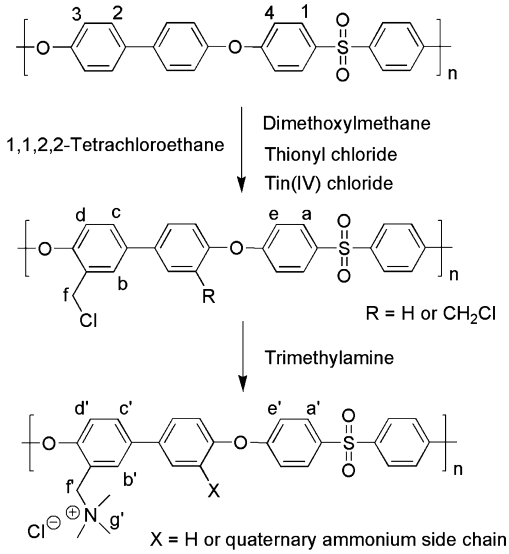

2.2.2. Quaternization of Chloromethylated Radel. 4 g of the chloromethylated Radel was dissolved in 160 mL of *N*,*N*′-dimethylacetamide under magnetic stirring in a 250 mL beaker. Then 20 mL of 30 wt % aqueous trimethylamine solution was added dropwise. The mixture was sealed with aluminum foil to prevent trimethylamine evaporation and stirred overnight at room temperature (25 °C). Next, the aluminum foil was removed and the mixture was stirred for 24 h to volatilize the excess trimethylamine. The mixture was transferred to a rotary evaporator to distill the solvents and leave a final solid product.

2.3. Membrane Preparation. The quaternary ammonium functionalized Radel samples were dissolved in *N*,*N*′-dimethylacetamide solution at approximately 8 wt/vol % and then cast onto glass plates, dried at 80 °C under atmosphere pressure for 24 h. The cast membranes were then peeled from the glass plate and immersed in 1 L of 1 M Na_2SO_4 solution for 24 h, followed by immersion in deionized water for 24 h with three DI water changes. The membranes were stored in deionized water until use.

2.4. Characterization. *2.4.1. Membrane Property Evaluation.* ^{1}H NMR was recorded on a Bruker AV-300 NMR instrument, and the chemical shifts were listed in parts per million (ppm) downfield from tetramethylsilane (TMS). The water uptake of the membranes was defined as weight ratio of the absorbed water to that of the dry membrane. The swelling ratio was described as the linear in-plane expansion ratio of the hydrated membrane compared to its dry state. The density of a membrane was the product of the mass of the membrane divided by its volume. Ionic conductivity was measured by two-probe electrochemical impedance spectroscopy (EIS) using a Solartron 1260A frequency response analyzer.[30] Samples were equilibrated in large excess of 1.4 M $VOSO_4$ + 2.0 M H_2SO_4 solution for 24 h before conductivity measurement. The VO^{2+} permeability measurements were conducted in a membrane-separated cell by filling vanadium solution into one reservoir and vanadium-blank solution with equivalent ionic strength into another reservoir using the standard procedure reported in the literature.[14,31] The amount of the vanadium permeated was detected by UV−vis spectroscopy using a Shimadzu UV-2600 spectrophotometer. The mechanical properties were measured on an Instron 5866 Universal Testing Machine at room temperature (25 °C). Specimens were cut into rectangles and immersed in deionized water prior to test. The crosshead speed was 10 mm $min.^{-1}$.

The ion exchange capacities (IECs) of the membranes were calculated from the ^{1}H NMR and confirmed by titration. For ^{1}H NMR

method, the degree of functionalization of the quaternary ammonium groups was calculated from the integral ratio of the methylene peak to the polymer backbone peaks; for the titration method, 0.2 g of membrane (Cl^- form) was immersed in 50 mL of 0.2 M $NaNO_3$ solution for 24 h and titrated with 0.1 M $AgNO_3$ using K_2CrO_4 as colorimetric indicator. The IEC was calculated via

$$\mathrm{IEC} = \frac{\Delta V_{\mathrm{AgNO_3}} C_{\mathrm{AgNO_3}}}{m_{\mathrm{d}}} \quad (1)$$

where m_d is the mass of the dry membrane, ΔV_{AgNO_3} is the consumed volume of $AgNO_3$ solution, and C_{AgNO_3} is the concentration of $AgNO_3$ solution.

2.4.2. Cell Performance. The VRFB setup was the same as our previous report.[10,32] The battery was composed of a symmetric cell consisting of two graphite current collectors, two carbon felt electrodes with an area of 10 cm^{-2}, and the membrane separator to isolate the anolyte and catholyte. The starting electrolyte was 1.4 M $VOSO_4$ + 2.0 M H_2SO_4. The electrolyte volume in the positive tank was 100 mL, while 50 mL of electrolyte was used in the negative tank. We used double the electrolyte volume in the positive tank because the oxidation of V^{4+} to V^{5+} is a one-electron reaction while the reduction of V^{4+} to V^{2+} is a two-electron reaction. The excess 50 mL of positive electrolyte was not removed during the test. Nitrogen was purged to the electrolyte tanks to protect the vanadium species from oxidation. All electrochemical measurements were conducted using a fully automated redox flow battery testing system (Scribner 857 Redox Flow Cell System). For charge/discharge experiments, a constant current program was used with an upper limit voltage of 1.7 V and a lower limit voltage of 0.7 V to determine the end of the charge/discharge processes under each current density studied. For polarization curve measurements, the current was scanned with the lower limit voltage of 0.2 V to determine the end of the polarization curve. The VRFBs were first fully charged at 80 mA cm^{-2}, then the discharge current was scanned from 0 A to 700 mA cm^{-2} with steps of 10 mA cm^{-2}. The hold time at each step was 30 s. The cell potential after 30 s was recorded and plotted against current density. The CE, VE, and EE of the cell were calculated from the following equations:

$$\mathrm{CE} = \frac{t_{\mathrm{d}}}{t_{\mathrm{c}}} \times 100\% \quad (2)$$

$$\mathrm{VE} = \frac{V_{\mathrm{d}}}{V_{\mathrm{c}}} \times 100\% \quad (3)$$

$$\mathrm{EE} = \mathrm{CE} \times \mathrm{VE} \quad (4)$$

where t_d is the discharging time, t_c is the charging time, V_d is the average discharging voltage, and V_c represents the average charging voltage.

3. RESULTS AND DISCUSSION

3.1. Membrane Synthesis and Properties. The chloromethylation of Radel was conducted with three different reaction times to obtain different degrees of functionalization, which were calculated from ^{1}H NMR spectroscopy of the chloromethylated Radel samples by taking the integral ratio of the chloromethyl proton peak (peak f, Figure 1) to the unfunctionalized Radel backbone proton peak (peak a, Figure 1). The degrees of functionalization for the products from 4, 6, and 10 h reaction times were found to be 0.84, 1.01, and 1.33 moles of chloromethyl groups per mole of polymer repeat unit, respectively. Due to the high reactivity of the chloromethyl groups with trimethylamine, the simple mixing of chloromethylated polymer and trimethylamine in solution quantitatively yielded quaternary ammonium groups. As can be seen in the ^{1}H NMR of QA-Radel in Figure 1, the chloromethyl proton peak of the chloromethylated Radel was completely replaced by

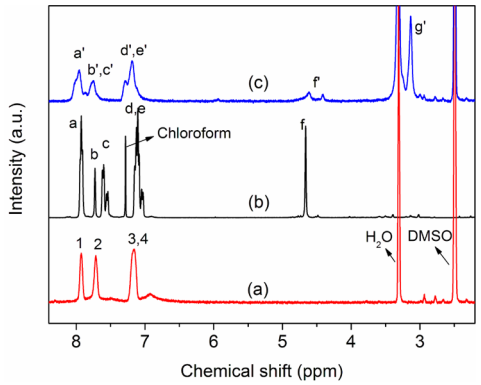

Figure 1. ^{1}H NMR spectra of (a) Radel in DMSO-d_6, (b) chloromethylated Radel in $CDCl_3$, and (c) QA-Radel in DMSO-d_6.

the methyl proton peak (peak g′) and methylene proton peak (peak f′) of the quaternary ammonium group. The integral ratio of peak g′ to peak f′ was close to 9:2, consistent with the composition of quaternary ammonium groups. Based on these ^{1}H NMR results, the IECs of the QA-Radel samples derived from the chloromethylated Radel precursors with 0.84, 1.01, and 1.33 degrees of functionalization were 1.7, 2.0, and 2.4 mequiv g^{-1}, respectively. These samples were named QA-Radel-1.7, QA-Radel-2.0, and QA-Radel-2.4.

Membranes with thicknesses in the range of 55−60 μm were obtained by solution casting. The basic membrane properties are listed in Table 1. The water uptake and swelling ratio increased monotonically with increasing IEC. These increases were attributed to the higher degree of hydrophilicity of the samples with greater IEC. The ionic conductivity of the samples increased as well with the increase in IEC. It is worthwhile to point out that the QA-Radel-2.4 sample showed much higher water uptake and swelling ratio than the other two IEC samples, while its conductivity only had a marginal increase. Thus, pushing the IEC to higher levels is not necessarily desirable as poor mechanical properties and large crossover can result due to the increased swelling. In membrane VO^{2+} permeability measurements, Table 1, the QA-Radel-2.4 exhibited large values similar to Nafion, which is not desirable due to severe self-discharge during cell operation.[14] The VO^{2+} permeability of the QA-Radel-2.0 was more than 1 order of magnitude lower than that of the QA-Radel-2.4 sample. VO^{2+} permeation across the QA-Radel-1.7 membrane was not detected during a 1-week permeation experiment. The promisingly low vanadium permeability of the QA-Radel-2.0 and QA-Radel-1.7 samples was likely due to the Donnan exclusion of vanadium cations by the positively charged quaternary ammonium groups in the membrane. The large swelling of the QA-Radel-2.4 decreased the ionic concentration in the sample and lowered the effective Donnan potential. By taking into account the gravimetric IEC and the water swelling and density of the membranes, the calculated ion concentrations in the samples were 1.7, 1.8, and 1.5 mequiv cm^{-3} for QA-Radel-1.7, QA-Radel-2.0, and QA-Radel-2.4, respectively, which supports a lower Donnan potential of the QA-Radel-2.4 sample.

The tensile properties of the QA-Radel membranes are shown in Figure 2. It can be seen that both the stress and strain decreased with increasing IEC. This is because the water uptake increased with increasing IEC, which plasticized the polymer and weakened the sample. For comparison, the tensile

dx.doi.org/10.1021/am401858r | ACS Appl. Mater. Interfaces 2013, 5, 7559−7566

Table 1. Physical Properties of QA-Radel Membranes and Nafion N212

sample	IEC_w from ^1H NMR (mequiv g^{-1})	IEC_w from titration (mequiv g^{-1})	IEC_v (mequiv cm^{-3})	water uptake (%)	swelling ratio (%)	conductivity (mS cm^{-1})	VO^{2+} permeability (m^2 s^{-1})
QA-Radel-1.7	1.7	1.7	1.7	16	7	24	
QA-Radel-2.0	2.0	2.0	1.8	29	12	41	3.7×10^{-14}
QA-Radel-2.4	2.4	2.5	1.5	73	23	49	2.9×10^{-12}
N212				28	14	44	3.2×10^{-12}

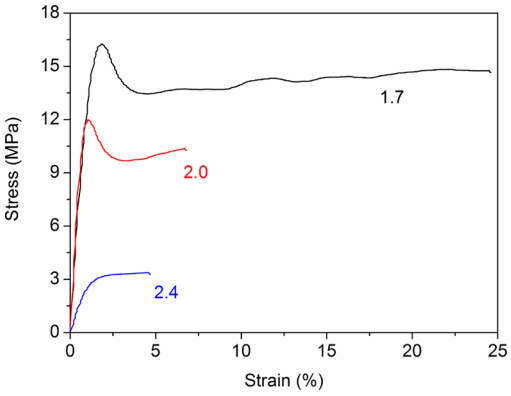

Figure 2. Tensile properties of QA-Radel membranes. Numbers in the figure represent the IECs (i.e., 1.7, 2.0, 2.4 mequiv g^{-1}) of the membranes.

properties of Nafion N212 were also measured under exactly the same condition and shown in Figure S1 (Supporting Information). It can be seen that Nafion had slightly higher yield stress than QA-Radel-2.4, but lower yield stress than QA-Radel-2.0 and QA-Radel-1.7. The unique tensile characteristics of Nafion is very high elongation at break, like a rubber, as compared to most thermoplastic ionomers based on poly(arylene ether)s.[33] Although the elongations at break for the QA-Radel samples were lower than Nafion, these AEMs were flexible and ductile for facile integration in test cells.

3.2. Cell Performance. The charge−discharge curves of the VRFBs assembled with different IEC QA-Radel membranes for a range of current densities are shown in Figure 3. The cell assembled with the QA-Radel-2.4 membrane had the shortest charge and discharge times among the three VRFB membranes tested, while the VRFB assembled with the QA-Radel-2.0 membrane had the longest charge and discharge times. The charge/discharge times under any given current density dictates the available charge/discharge capacities. For the VRFB assembled with the QA-Radel-2.4 membrane, the high VO^{2+} permeability of the membrane led to significant crossover of the vanadium electrolytes, resulting in the lowest charge/discharge capacity of the cells tested. For the VRFB assembled with the QA-Radel-1.7 membrane, the low VO^{2+} permeation of the membrane was associated with the lowest ionic conductivity among the three QA-Radel samples, causing the highest ohmic polarization of the batteries and therefore the lowest utilization efficiency of the active vanadium electrolyte species. The combination of the low VO^{2+} permeability and low ionic conductivity of QA-Radel-1.7 rendered a battery with

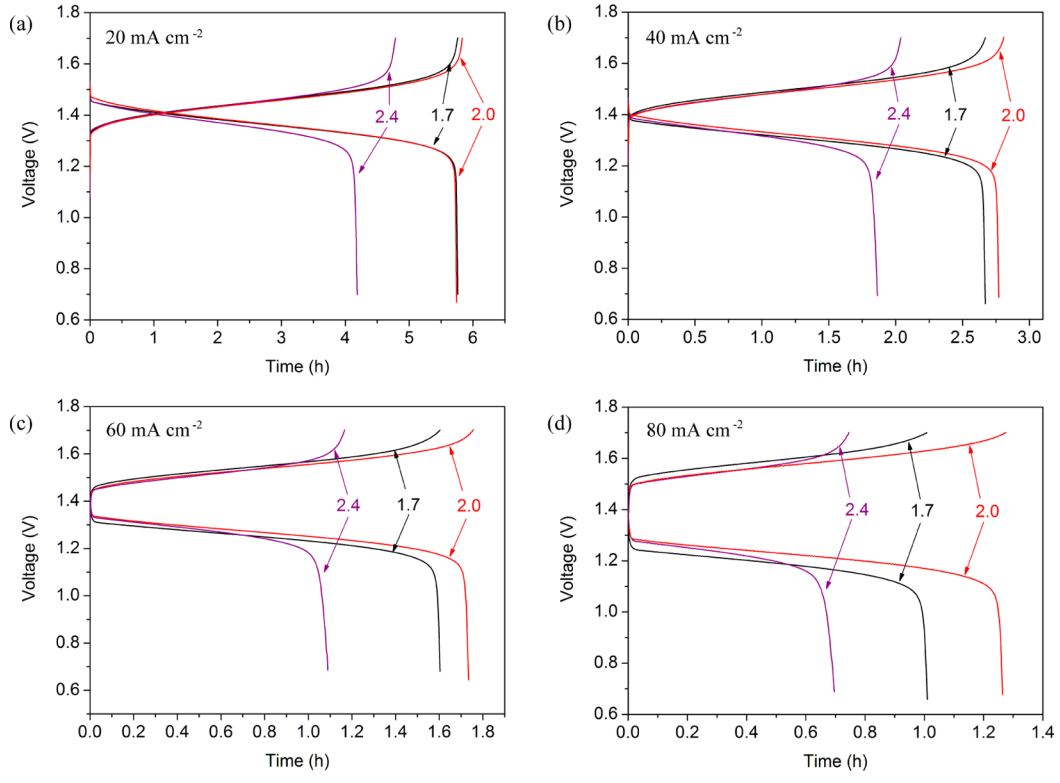

Figure 3. Charge−discharge curves of the VRFBs assembled with different QA-Radel membranes at 20 mA cm^{-2} (a), 40 mA cm^{-2} (b), 60 mA cm^{-2} (c), and 80 mA cm^{-2} (d).

dx.doi.org/10.1021/am401858r | ACS Appl. Mater. Interfaces 2013, 5, 7559−7566

intermediate charge/discharge capacities compared to cells incorporating the other two membrane samples. The QA-Radel-2.0 membrane turned out to be the best membrane in this study for the VRFB application, suggesting that there was an optimal relationship between VO^{2+} permeability and ionic conductivity for the AEM samples in VRFBs. It can also be seen in Figure 3 that with increasing current density, the charge voltage increased while the discharge voltage decreased for all the VRFBs. This difference was attributed to the higher ohmic polarization of the batteries at higher current density. The charge/discharge times decreased as the current density was raised, as expected, due to the fixed amount of electrolyte in the cell.

The Coulombic efficiencies (CEs) of the VRFBs assembled with QA-Radel samples are shown in Figure 4 with CE data for

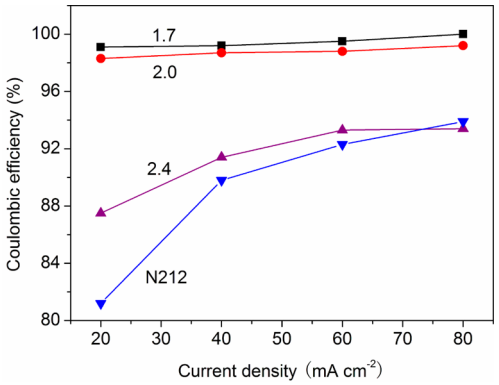

Figure 4. Coulombic efficiencies of the VRFBs assembled with the QA-Radel samples and Nafion N212.

a Nafion N212 membrane for comparison. For the QA-Radel samples, the VRFB assembled with the QA-Radel-1.7 membrane had the highest CEs while the VRFB assembled with the QA-Radel-2.4 membrane had the lowest CEs under all the current densities tested in this work, in good agreement with the VO^{2+} permeability results. CE describes the efficiency of round-trip storage and release of electrons from the cell redox reactions. The vanadium ion crossover and unwanted side reactions, such as electrode corrosion that consumes electrons or ions, may cause Coulombic losses.[10] Since the VRFBs tested were of identical construction except the IECs of the QA-Radel separators, the possible side reactions during the charge/discharge processes should be similar for all experiments in this study. Therefore, the ion crossover was the dominant factor that determined the relative CEs of the VRFBs. This explains why the CE decreased with the increasing VO^{2+} permeability of the membrane separators. With an increase in current density, the CEs increased monotonically. This increase in CE was attributed to the shorter time for vanadium crossover at higher current density during the charge/discharge processes since the cycle time was significantly decreased. The CE of the VRFB assembled with the QA-Radel-1.7 membrane at 80 mA cm^{-2} was nearly 100%, similar to our previously reported partially fluorinated anion exchange membrane with extremely low vanadium crossover.[23] This result suggested that possible side reactions such as V^{5+} oxidation of the polymeric membrane or the carbon-based electrodes were minimal under the operational conditions of the cells in this work and the losses approached the instrumental error from small fluctuations of the applied currents during the galvanostatic charge/discharge processes. The VRFB assembled with N212 suffered from low CEs as shown in Figure 4, in good agreement with previous studies.[3,17]

The voltage efficiencies (VEs) of the VRFBs at different current densities are shown in Figure 5. For the QA-Radel

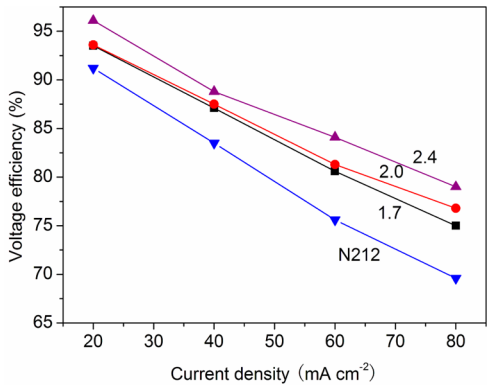

Figure 5. Voltage efficiencies of the VRFBs assembled with the QA-Radel samples and Nafion N212.

samples, the VE increased with increasing IEC of the membrane used in the VRFB at any current density, consistent with the membranes' trend in ionic conductivity. Therefore, increasing the IEC of the membrane was advantageous for the VE of the VRFBs while it was detrimental to the CE of the batteries. A further increase of the IEC beyond 2.4 mequivg^{-1} may result in reduced VE due to large crossover voltage loss, which was not addressed in this study.[10] With the increase in current density, the VE for all the VRFBs decreased gradually due to the increasing ohmic polarization loss of the cells. It can be seen in Figure 5 that the difference in VE for the three VRFBs was only a few percent, while the ionic conductivity of the QA-Radel membranes varied by more than double. This result suggested that the resistance of the membrane was not the main contribution to the total resistance of the cells in this study. Surprisingly, the VEs for VRFB assembled with N212 were the lowest in Figure 5 while the conductivity of N212 was reasonably high (Table 1). This result suggested that the large vanadium permeability of N212 reduced its cell voltage. This effect was different than what was observed in the QA-Radel samples where the lowest conductivity QA-Radel-1.7 membrane had the lowest VE and the highest permeability QA-Radel-2.4 sample had reasonable VE, in line with its high conductivity. There could be in situ resistance losses for Nafion that are not accounted for when comparing ex-situ conductivity measurements with battery performance, which would cause a greater than expected VE decrease. It is also possible that the static VO^{2+} permeability in membrane-separated diffusion cells does not reflect the vanadium crossover of the membranes in an operating battery. The permeability of other vanadium species is important, in addition to VO^{2+}, especially for different types of membranes since the relative trend of various vanadium species to VO^{2+} permeability may be different. In-cell measurements of membrane resistance and vanadium species crossover are needed to help gain insights into in-cell membrane processes.

The product of CE and VE is energy efficiency (EE), which is used to describe the ratio of the output and input energy of the cell. Self-discharge (vanadium crossover), side reactions, and polarization are the main sources of energy loss in VRFBs.[3]

From Figure 6, it can be seen that the VRFB assembled with the QA-Radel-2.4 membrane had the lowest EE at all the

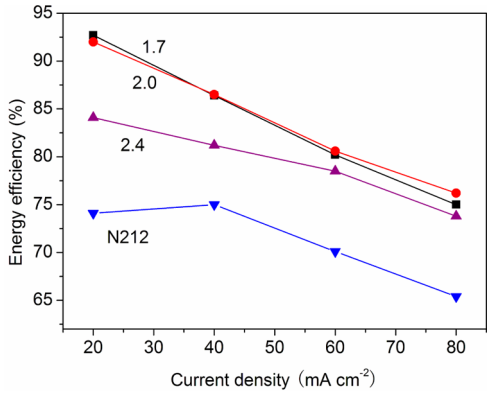

Figure 6. Energy efficiencies of the VRFBs assembled with the QA-Radel membranes and Nafion N212.

current densities tested for QA-Radel systems. The VRFB assembled with the QA-Radel-1.7 membrane had the highest EE at low current densities (e.g., 20 and 40 mA cm^{-2}) while the VRFB assembled with the QA-Radel-2.0 membrane had the highest EE at high current densities (60 and 80 mA cm^{-2}). Therefore, membranes with high VO^{2+} permeability such as QA-Radel-2.4 are not suitable for VRFBs. However, membranes with low VO^{2+} permeability and low ionic conductivity such as QA-Radel-1.7 are promising for VRFBs operated at low current densities and membranes with low VO^{2+} permeability and high ionic conductivity such as QA-Radel-2.0 are promising for VRFBs operated at high current densities. The EEs for the VRFB assembled with N212 membrane were the lowest of all samples tested, Figure 6, further highlighting the limitations of using N212 in high-performance VRFBs.

The influence of the membrane IEC on the cycling performance of the VRFBs was investigated. As shown in Figure 7, the initial discharge capacities of the VRFBs varied

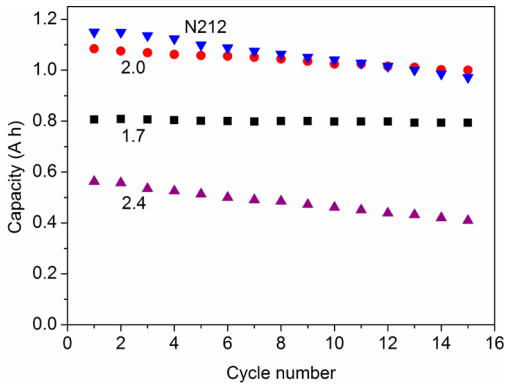

Figure 7. Discharge capacities of the VRFBs as a function of cycle number at 80 mA cm^{-2}.

due to the different discharge times at the same current density in Figure 3, which also reflected different utilization rates of the vanadium species or charge depth of the batteries. During cycling, the capacity of the VRFB assembled with the QA-Radel-1.7 membrane exhibited the smallest decline while the capacity of the VRFB assembled with QA-Radel-2.4 decayed most rapidly, as is consistent with the CE of the single cycle performance where QA-Radel-1.7 had the highest CE and QA-Radel-2.4 had the lowest CE. The IEC of the QA-Radel samples influenced the VO^{2+} permeability of the membranes, which was reflected in the CE of the VRFBs in the cell output performance and on the capacity fade of the VRFBs in cell cycling tests. In the normalized capacities of the VRFBs during cycling tests, Figure 8, it is clear that the rate of capacity fade

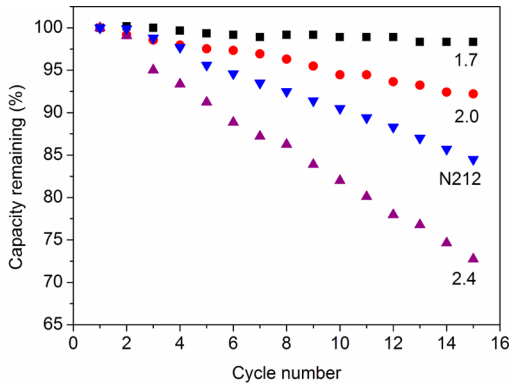

Figure 8. Normalized discharge capacities of the VRFBs as a function of cycle number at 80 mA cm^{-2}.

increased with increasing membrane IEC. After 15 cycles, the capacity of the VRFB assembled with a QA-Radel-2.4 membrane maintained 73% of its initial capacity while the capacity of the VRFB assembled with QA-Radel-1.7 maintained 98% of its initial capacity. Therefore, careful control of the membrane IEC was critically important for battery cycling performance to optimize the membrane conductivity and permeability.

While the QA-Radel-2.4 sample had slightly lower VO^{2+} permeability than N212, its capacity decay rate was higher than N212 as shown in Figure 8, which highlights some discrepancy between ex situ materials characterization and in situ battery testing. Therefore, a technique that can probe the amount of vanadium permeation and the different vanadium species under applied currents is critical for the study of VRFB membranes, especially when comparing different types of membranes. Since the QA-Radel samples and N212 are oppositely charged polymers, the connection between the static VO^{2+} permeability and the dynamic vanadium permeability in real battery systems may differ, which would result in different cell performance that is difficult to predict from ex-situ measured materials properties.

The polarization curves of the VRFBs assembled with the QA-Radel samples are shown in Figure 9, with the polarization curve of the VRFB assembled with a Nafion N212 membrane for comparison. It can be seen that the voltage of the VRFB assembled with the QA-Radel-2.4 membrane showed slightly poorer performance than the VRFB assembled with N212. The voltage of the VRFB assembled with the QA-Radel-1.7 membrane maintained higher current density than that of the VRFB with a N212 separator, while the voltage of the VRFB with the QA-Radel-2.0 membrane displayed the highest current density (420 mA cm^{-2}). The discharge voltage of the VRFB can be represented as $V = E - \Delta V_{act} - \Delta V_{ohm} - \Delta V_{trans} - \Delta V_{cross}$, where E is the theoretical open circuit voltage of the cell, ΔV_{act} is the voltage loss caused by activation, ΔV_{ohm} is the voltage loss caused by ohmic loss (or iR loss where i is current and R is resistance), ΔV_{trans} is the voltage loss caused by mass transport, and ΔV_{cross} is the voltage loss caused by electrolyte crossover.

dx.doi.org/10.1021/am401858r | ACS Appl. Mater. Interfaces 2013, 5, 7559−7566

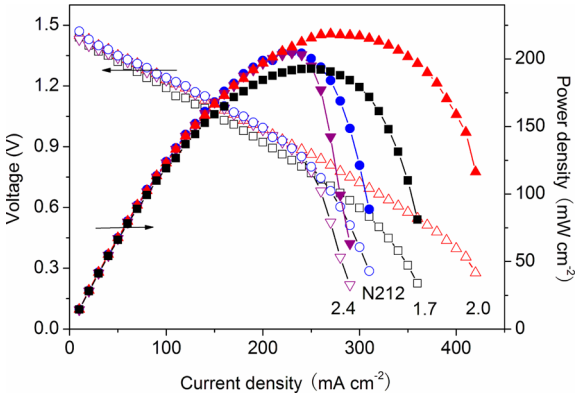

Figure 9. Polarization curves and power densities of the VRFBs as a function of current density.

The properties of membrane have a direct impact on the terms of ΔV_{ohm} and ΔV_{cross} though membrane resistance and VO^{2+} crossover, respectively. Therefore, the QA-Radel-2.0 sample had the best balance of properties for high current density operation. The highest power density achieved for these VRFBs was 218 mW cm^{-2}, which was obtained at a current density of 270 mA cm^{-2} using the QA-Radel-2.0 membrane. While this performance was lower than the highest power density of our previously reported VRFB using an IEC- and thickness-optimized proton exchange membrane,[10] this result still was higher than the maximum power density of the VRFB assembled with N212 and demonstrated good prospects for employing optimized anion exchange membranes in VRFBs.

Membrane stability is another important concern for VRFBs.[34,35] It was found that the stability of anion exchange membranes was higher than the stability of proton exchange membranes in V^{5+} electrolyte soaking tests, likely due to the low concentration of vanadium cations in the membrane.[36] We believe that the lifetime of the investigated QA-Radel samples should be similar to other anion exchange membranes based on quaternary ammonium functionalized poly(arylene ether)s since they had similar chemical structures.[10] Long-term cycle testing is still ongoing in our lab and detailed degradation mechanisms for in situ and ex-situ testing will be proposed in the future.

4. CONCLUSIONS

Quaternary ammonium functionalized Radel (QA-Radel) membranes with three different IECs (1.7, 2.0, and 2.4 mequiv g^{-1}) were synthesized and evaluated in VRFBs. The ionic conductivity of the QA-Radel samples after equilibration in 1.4 M $VOSO_4$ + 2.0 M H_2SO_4 solution was of the same order as that of an electrolyte-equilibrated Nafion N212 membrane, while the VO^{2+} permeability of the QA-Radel samples was significantly lower than that of the N212 except the QA-Radel with an IEC of 2.4 mequiv g^{-1}. Increasing the IEC of the QA-Radel samples increased both the ionic conductivity and the VO^{2+} permeability of the membranes. The ionic conductivity of the membranes influenced the voltage efficiency of the battery while the VO^{2+} permeability of the membranes affected the Coulombic efficiency of the cells. It was found that the VRFB assembled with QA-Radel-1.7 membrane had the highest energy efficiency at 20 and 40 mA cm^{-2} charge/discharge current densities, while the VRFB assembled with the QA-Radel-2.0 separator had the highest energy efficiency at 60 and 80 mA cm^{-2}. The VRFB assembled with the QA-Radel-2.4 membrane exhibited the lowest energy efficiency at all the current densities tested because of the high VO^{2+} permeability of the sample. Increasing the membrane IEC also resulted in faster capacity fade during cell cycling tests. Due to the best balance of ionic conductivity and VO^{2+} permeability in QA-Radel-2.0, the VRFB with this membrane showed the highest power density of all samples in this study (218 mW cm^{-2}), more than the maximum power density of the VRFB assembled with N212.

■ ASSOCIATED CONTENT

Ⓢ Supporting Information

Figure showing the tensile properties of Nafion N212. This material is available free of charge via the Internet at http://pubs.acs.org.

■ AUTHOR INFORMATION

Corresponding Author

*(M.A.H.) Tel.: +1 814 867 1847. Fax: +1 814 865 2917. E-mail: hickner@matse.psu.edu. (E.C.K.) Tel.: +1 215 895 5871. Fax: +1 215 895 1478. E-mail: eck32@drexel.edu

Notes

The authors declare no competing financial interest.

■ ACKNOWLEDGMENTS

The work was supported by the Office of Electricity (OE Delivery & Energy Reliability (OE), U.S. Department of Energy (DOE) under Contract DE-AC05-76RL01830. We also acknowledge the support from the Southern Pennsylvania Ben Franklin Commercialization Institute (Grant #001389-002) and the Virginia S. and Philip L. Walker, Jr. Faculty Fellowship to M.A.H. from the College of Earth and Mineral Sciences at The Pennsylvania State University.

■ REFERENCES

(1) Skyllas-Kazacos, M.; Grossmith, F. *J. Electrochem. Soc.* **1987**, *134*, 2950−2953.
(2) Rychcik, M.; Skyllas-Kazacos, M. *J. Power Sources* **1988**, *22*, 59−67.
(3) Chen, D.; Wang, S.; Xiao, M.; Meng, Y. *J. Power Sources* **2010**, *195*, 2089−2095.
(4) Li, X.; Zhang, H.; Mai, Z.; Zhang, H.; Vankelecom, I. *Energy Environ. Sci.* **2011**, *4*, 1147−1160.
(5) Schwenzer, B.; Zhang, J.; Kim, S.; Li, L.; Liu, J.; Yang, Z. *ChemSusChem* **2011**, *4*, 1388−1406.
(6) Weber, A. Z.; Mench, M. M.; Meyers, J. P.; Ross, P. N.; Gostick, J. T.; Liu, Q. *J. Appl. Electrochem.* **2011**, *41*, 1137−1164.
(7) Wen, J.; Yu, Y.; Chen, C. *Mater. Express* **2012**, *2*, 197−212.
(8) Parasuraman, A.; Lim, T. M.; Menictas, C.; Shyllas-Kazacos, M. *Electrochim. Acta* **2013**, *101*, 27−40.
(9) Skyllas-Kazacos, M.; Rychcik, M.; Robins, R. G.; Fane, A. G.; Green, M. A. *J. Electrochem. Soc.* **1986**, *133*, 1057−1058.
(10) Chen, D.; Hickner, M. A.; Agar, E.; Kumbur, E. C. *J. Membr. Sci.* **2013**, *437*, 108−113.
(11) Zhang, H.; Zhang, H.; Li, X.; Mai, Z.; Wei, W.; Li, Y. *J. Power Sources* **2012**, *217*, 309−315.
(12) Ma, J.; Wang, Y.; Peng, J.; Qiu, J.; Xu, L.; Li, J.; Zhai, M. *J. Membr. Sci.* **2012**, *419−420*, 1−8.
(13) Chen, D.; Wang, S.; Xiao, M.; Meng, Y. *Energy Environ. Sci.* **2010**, *3*, 622−628.
(14) Chen, D.; Kim, S.; Li, L.; Yang, G.; Hickner, M. A. *RSC Adv.* **2012**, *2*, 8087−8094.
(15) Chen, D.; Kim, S.; Sprenkle, V.; Hickner, M. A. *J. Power Sources* **2013**, *231*, 301−306.

(16) Wang, N.; Peng, S.; Wang, H.; Li, Y.; Liu, S.; Liu, Y. *Electrochem. Commun.* **2012**, *17*, 30−33.
(17) Teng, X.; Zhao, Y.; Xi, J.; Wu, Z.; Qiu, X.; Chen, L. *J. Membr. Sci.* **2009**, *341*, 149−154.
(18) Trogadas, P.; Pinot, E.; Fuller, T. F. *Electrochem. Solid-State Lett.* **2012**, *15*, A5−A8.
(19) Teng, X.; Sun, C.; Dai, J.; Liu, H.; Su, J.; Li, F. *Electrochim. Acta* **2013**, *88*, 725−734.
(20) Vijayakumar, M.; Schwenzer, B.; Kim, S.; Yang, Z.; Thevuthasan, S.; Liu, J.; Graff, G. L.; Hu. *Solid State Nucl. Magn. Reson.* **2012**, *42*, 71−80.
(21) Chen, D.; Wang, S.; Xiao, M.; Han, D.; Meng, Y. *J. Power Sources* **2010**, *195*, 7701−7708.
(22) Ling, X.; Jia, C.; Liu, J.; Yan, C. *J. Membr. Sci.* **2012**, *415−416*, 306−312.
(23) Chen, D.; Hickner, M. A.; Agar, E.; Kumbur, E. C. *Electrochem. Commun.* **2013**, *26*, 37−40.
(24) Mohammadi, T.; Skyllas-Kazacos, M. *J. Power Sources* **1996**, *63*, 179−186.
(25) Zhang, H.; Zhang, H.; Zhang, F.; Li, X.; Li, Y.; Vankelecom, I. *Energy Environ. Sci.* **2013**, *6*, 776−781.
(26) Xi, J.; Wu, Z.; Teng, X.; Zhao, Y.; Chen, L.; Qiu, X. *J. Mater. Chem.* **2008**, *18*, 1232−1238.
(27) Hu, G.; Wang, Y.; Ma, J.; Qiu, J.; Peng, J.; Li, J.; Zhai, M. *J. Membr. Sci.* **2012**, *407−408*, 184−192.
(28) Seo, S.; Kim, B.; Sung, K.; Shim, J.; Jeon, J.; Shin, K.; Shin, S.; Yun, S.; Lee, J.; Moon, S. *J. Membr. Sci.* **2013**, *428*, 17−23.
(29) Geise, G. M.; Falcon, L. P.; Freeman, B. D.; Paul, D. R. *J. Membr. Sci.* **2012**, *423−424*, 195−208.
(30) Fujimoto, C. Y.; Hickner, M. A.; Cornelius, C. J.; Loy, D. A. *Macromolecules* **2005**, *38*, 5010−5016.
(31) Mohammadi, T.; Skyllas-Kazacos, M. *J. Membr. Sci.* **1995**, *107*, 35−45.
(32) Knehr, K. W.; Agar, E.; Dennison, C. R.; Kalidindi, A. R.; Kumbur, E. C. *J. Electrochem. Soc.* **2012**, *159*, A1−A14.
(33) Chen, D.; Wang, S.; Xiao, M.; Meng, Y.; Hay, A. S. *J. Mater. Chem.* **2011**, *21*, 12068−12077.
(34) Chen, D.; Hickner, M. A. *Phys. Chem. Chem. Phys.* **2013**, *15*, 11299−11305.
(35) Mohammadi, T.; Skyllas-Kazacos, M. *J. Appl. Electrochem.* **1997**, *27*, 153−160.
(36) Mai, Z.; Zhang, H.; Zhang, H.; Xu, W.; Wei, W.; Na, H.; Li, X. *ChemSusChem* **2013**, *6*, 328−335.